Atmos. Chem. Phys., 17, 531–549, 2017
www.atmos-chem-phys.net/17/531/2017/
doi:10.5194/acp-17-531-2017

Atmospheric Chemistry and Physics
Open Access
EGU

Diurnal variability of the atmospheric boundary layer height over a tropical station in the Indian monsoon region

Sanjay Kumar Mehta[1], Madineni Venkat Ratnam[2], Sukumarapillai V. Sunilkumar[3], Daggumati Narayana Rao[1], and Boddapaty V. Krishna Murthy[1]

[1]SRM Research Institute, SRM University, Kattankulathur 603203, India
[2]National Atmospheric Research Laboratory, Gadanki 517112, India
[3]Space Physics Laboratory (SPL), VSSC, Trivandrum 695022, India

Correspondence to: Sanjay Kumar Mehta (sanjaykumar.r@res.srmuniv.ac.in, ksanjaym@gmail.com)

Received: 21 June 2016 – Published in Atmos. Chem. Phys. Discuss.: 4 July 2016
Revised: 14 December 2016 – Accepted: 17 December 2016 – Published: 11 January 2017

Abstract. The diurnal variation of atmospheric boundary layer (ABL) height is studied using high-resolution radiosonde observations available at 3 h intervals for 3 days continuously from 34 intensive campaigns conducted during the period December 2010–March 2014 over a tropical station Gadanki (13.5° N, 79.2° E; 375 m), in the Indian monsoon region. The heights of the ABL during the different stages of its diurnal evolution, namely, the convective boundary layer (CBL), the stable boundary layer (SBL), and the residual layer (RL) are obtained to study the diurnal variabilities. A clear diurnal variation is observed in 9 campaigns out of the 34 campaigns. In 7 campaigns the SBL did not form in the entire day and in the remaining 18 campaigns the SBL formed intermittently. The SBL forms for 33–55 % of the time during nighttime and 9 and 25 % during the evening and morning hours, respectively. The mean SBL height is within 0.3 km above the surface which increases slightly just after midnight (02:00 IST) and remains almost constant until the morning. The mean CBL height is within 3.0 km above the surface, which generally increases from morning to evening. The mean RL height is within 2 km above the surface which generally decreases slowly as the night progresses. The diurnal variation of the ABL height over the Indian region is stronger during the pre-monsoon and weaker during winter season. The CBL is higher during the summer monsoon and lower during the winter season while the RL is higher during the winter season and lower during the summer season. During all the seasons, the ABL height peaks during the afternoon (∼ 14:00 IST) and remains elevated until evening (∼ 17:00 IST). The ABL suddenly collapses at 20:00 IST and increases slightly in the night. Interestingly, it is found that the low level clouds have an effect on the ABL height variability, but the deep convective clouds do not. The lifting condensation level (LCL) is generally found to occur below the ABL for the majority of the database and they are randomly related.

1 Introduction

The atmospheric boundary layer (ABL) is the lowest layer of the troposphere in which the flow field is directly influenced by the interaction of the Earth's surface at a response timescale of about an hour or less (Stull, 1988; Garratt, 1994). The importance of the ABL stems from the fact that it is the gateway for the pollutants and anthropogenic emissions, moisture, heat, and momentum fluxes to the free atmosphere. Rapid transport in the ABL takes place in order to achieve the radiative balance between the surface and the free atmosphere. The ABL is the largest sink for atmospheric kinetic energy. The ABL height is a key parameter, providing a length scale for the vertical extent and concentration of atmospheric pollutants, convective activity, and cloud and fog formation (Deardorff, 1972; Holtslag and Nieuwstadt, 1986; Seibert et al., 2000; Konor et al., 2009). The diurnal variability is a dominant feature of the ABL, which plays an important role in the exchanges of heat, momentum, moisture, and chemical constituents between the surface and free atmosphere.

Depending on the physical process, the diurnal pattern of the ABL is mainly classified into three major layers: the convective boundary layer (CBL), the stable boundary layer (SBL), and the residual layer (RL) (Stull, 1988; Garratt, 1994). The CBL evolves during the daytime just after the sunrise due to convective turbulence (thermals of warmer air) associated with entrainment zone, a stable layer, on its top. Just before the sunset and during night, as the thermals cease to develop, the CBL collapses and the SBL forms due to rapid cooling of the surface. Even though thermals cease to develop during nighttime, the mean state variables remain nearly the same as the former CBL, creating the RL associated with capping inversion layer, a stable layer, on its top. Thus, the RL is disconnected from the ground by underlying SBL having no source of turbulence generation for its maintenance; rather, turbulence decays homogeneously in all directions. One aspect of the RL that has been pointed out as being important for the diurnal evolution of the ABL is that it provides the potential for "explosive growth" of the ABL as a CBL forms in the morning and grows into the RL. Generally, the mean ABL height lies between 0.03 and 3.0 km above the surface (Stull, 1988). However, the CBL can be as high as ~ 5.0 km during a midsummer day in low-latitude deserts and as low as ~ 0.5 km over the ocean. The SBL height generally is less than 0.5 km above the surface (Garratt, 1992).

The daytime surface flux (the convectively induced turbulence) due to solar heating is stronger than nighttime surface flux (wind-induced turbulence) due to surface friction, causing diurnal variation in the ABL. However, the diurnal variabilities of the ABL is not only determined by the variations in the surface fluxes, but also by the meteorological conditions such as the presence of clouds, horizontal advection of air, and subsidence aloft. These forcings considerably affect turbulence development and the growth of the ABL. For example, the presence of clouds greatly influences the turbulent structure due to local radiative heating or cooling. The diurnal variation is generally strong, mainly over land in the absence of any upper level cloud and at the time of year when surface temperatures are the highest (Angevine et al., 2001).

The ABL height is often determined from the vertical profiles of temperature, humidity, and wind components obtained from radiosonde measurements (Schmid and Niyogi, 2012). Most of the routine radiosondes only operate twice a day at 00:00 and 12:00 UTC, which are not suited well to study the diurnal variations of the ABL height. Thus, there have been only a few studies on diurnal variability of the ABL height (Angevine et al., 2001) mainly due to non-availability of the required measurements with adequate time resolution. High-resolution radiosondes launched at sufficiently close time intervals (less than 1 h) can provide direct information on diurnal variability of ABL height. Liu and Liang (2010) studied the climatology of the ABL height diurnal cycle, using fine-resolution soundings launched at intervals ranging from 1 to 12 h collected in 14 major field campaigns around the world. They found a strong diurnal cycle, both over land and oceans, whereas the cycle is weak over ice-covered regions. Seidel et al. (2010), using routine radiosondes over the globe, found significant differences in day and night ABL heights. In an another study, Seidel et al. (2012) reported the seasonal pattern in the diurnal cycle of the ABL using 3-hourly ERA-Interim data and 6-hourly climate models outputs over the continental United States and Europe.

There are several case studies focusing on the diurnal structure of the boundary layer and the mechanism responsible for its formation over different regions of the globe. Brill and Albrecht (1982) presented the diurnal variation of the cloud fraction and trade-wind inversion base height using the data collected from various ships and aircraft. May et al. (2012) have studied the diurnal variation of convection, cloud, radiation, and boundary layer structure in the coastal monsoon environment (Darwin, Australia). Santanello et al. (2007) have studied the feedback of soil moisture dryness on the development of the convective boundary layer over the southern Atmospheric Research Measurement Program Southern Great Plains Cloud and Radiation Testbed (ARM-CART) sites. During a clear sky day, Hashiguchi et al. (1995a) observed boundary layer radar echo indicating the ABL height. Hashiguchi et al. (1995b) further observed that the boundary layer radar detects diurnal variation of the ABL both at the equatorial and midlatitude regions.

Recently, various remote sensing systems such as lidar (Tucker et al., 2009), sodar (Shravan Kumar and Anandan, 2009), wind profiler (Kumar and Jain, 2006; Bianco et al., 2011), Radio Acoustic Sounding System (RASS) (Clifford et al., 1994; Chandrasekhar Sarma et al., 2008), and ceilometer (van der Kamp and McKendry, 2010) have been developed for continuous direct measurements or estimates to study the diurnal variation of the ABL height (Seibert et al., 2000). Sodar can generally provide the SBL height but not always the CBL height due to inadequate height coverage. The lidars make use of aerosol extinction profiles and can provide information on diurnal variability of the ABL height. Using a network of wind profilers located in California's Central Valley, Bianco et al. (2011) studied the diurnal evolution of the CBL and reported that the CBL attains maximum height 3–4 h before the sunset. A few studies on the different ABL regimes (CBL and SBL) and their evening transition have been carried out using various remote sensing instruments located at Gadanki (Kumar and Jain, 2006; Basha and Ratnam, 2009; Kumar et al., 2012; Sandeep et al., 2015). These studies show that the mean CBL height is within 3.5 km and the mean SBL height lies below 0.6 km above the surface and their transition from the CBL to the SBL occurs about 1.5 h before the sunset. However, the complete diurnal variation of the ABL height has not been reported either using single instrument or a combination of two or more in the above-mentioned studies.

Over Gadanki (13.45° N, 79.2° E), a tropical location in the Indian monsoon region, high-resolution GPS radiosonde

Table 1. List of 3-day campaigns conducted during the period December 2010–March 2014. Total number of observations, rejection of bad quality data, the SBL, the CBL, and the RL are listed for each campaign. Shaded regions with italic fonts indicate campaigns with more than 90 % of the SBL defined. Bold indicates those campaigns where SBL is not defined and the rest when the SBL occur intermittently. Cloud top temperature (CTH) relative to ABL are also listed.

		No. of observations					
SN	Period	Total	Rejected	SBL	CBL	RL	CTH–ABL
1	*28–31 Dec 2010*	*24*	*0*	*10*	*12*	*12*	*±1.5*
2	*17–20 Jan 2011*	*24*	*0*	*14*	*10*	*6*	*−2.0–1.0*
3	*8–11 Feb 2011*	*24*	*0*	*14*	*11*	*7*	*−2.0–1.0*
4	**26–29 Apr 2011**	**24**	**2**	**0**	**11**	**10**	**−1.0–2.0**
5	18–21 May 2011	24	1	5	8	9	−1.0–7.0
6	**20–23 Jun 2011**	**24**	**0**	**0**	**12**	**12**	**−1.5–1.0**
7	**21–24 Jul 2011**	**24**	**0**	**0**	**12**	**12**	**−1.5–2.0**
8	17–20 Aug 2011	24	1	5	10	9	−1.5–1.0
9	*12–15 Sep 2011*	*24*	*1*	*11*	*12*	*8*	*±2.0*
10	12–15 Oct 2011	12	2	6	5	3	±0.5
11	*14–17 Nov 2011*	*24*	*0*	*13*	*12*	*12*	*−2.0–0.0*
12	8–11 Dec 2011	23	1	7	11	11	−2.0–8.0
13	18–21 Jan 2012	17	1	8	7	9	±2.0
14	*23–26 Feb 2012*	*22*	*0*	*13*	*10*	*11*	*−1.5–2.0*
15	**29 Mar–1 Apr 2012**	**23**	**0**	**0**	**12**	**11**	**−1.0–4.0**
16	1–4 Apr 2012	24	0	9	11	7	0.5–2.5
17	29 May–1 Jun 2012	23	0	6	12	11	−0.5–1.5
18	26–29 Jun 2012	23	0	8	10	8	−1.0–2.5
19	24–27 Jul 2012	24	2	4	11	11	−1.5–1.0
20	21–24 Aug 2012	23	0	8	10	6	−1.5–2.5
21	12–15 Sep 2012	23	0	7	11	8	−0.5–2.0
22	3–6 Oct 2012	21	0	6	11	10	±0.5
23	5–8 Nov 2012	12	1	2	6	5	±0.5
24	21–24 May 2013	22	1	6	10	10	−1.0–2.5
25	17–20 Jun 2013	24	0	2	12	12	−1.0–3.5
26	15–18 Jul 2013	24	0	5	12	12	−1.0–2.0
27	26–29 Aug 2013	24	0	5	11	7	−1.5–0.5
28	23–26 Sep 2013	24	0	4	11	6	±1.5
29	28–31 Oct 2013	21	0	6	11	9	−2.0–5.0
30	**21–24 Nov 2013**	**19**	**2**	**0**	**8**	**9**	**−2.0–5.0**
31	*18–21 Dec 2013*	*24*	*0*	*11*	*12*	*12*	*1.0–11.0*
32	**27–30 Jan 2014**	**24**	**0**	**0**	**12**	**12**	**−0.5–(−2.0)**
33	**24–27 Feb 2014**	**24**	**0**	**0**	**12**	**12**	**−2.0–0.5**
34	*25–28 Mar 2014*	*24*	*1*	*12*	*12*	*11*	*−1.0–7.0*
	Total	764	17	207	360	320	

launches were carried out at 3 h intervals for 3 consecutive days each month during the period December 2010–March 2014. Making use of this dataset, for the first time the complete diurnal evolution and variability of the ABL height and its seasonal pattern are studied and the results are presented in this paper. The objectives of present study are to (i) document the boundary layer heights from radiosonde data, (ii) study the evolution of the different ABL regimes such as the CBL, SBL, and RL, and (iii) qualitatively describe the nature of the ABL in the presence of clouds. Section 2 describes the data and methodology, results are presented in Sect. 3, and in Sect. 4 the discussion and concluding remarks are presented.

2 Data and method of analysis

2.1 GPS radiosonde data

As part of Tropical Tropopause Dynamics (TTD) experiment under Climate and Weather of Sun–Earth System India (CAWSES-India) program, intensive campaigns of high-resolution GPS radiosonde were conducted to study the diurnal variability of the ABL over a tropical sta-

tion, Gadanki, located at 375 m above mean sea level. The radiosondes were launched at 3 h intervals for 3 consecutive days in each month from December 2010 to March 2014, except during March 2011, December 2012, January–February, and April 2013. Each campaign started at 11:00 IST (UTC +05:30) on day 1 and ended at 08:00 IST on the day 4. Table 1 shows the dates of radiosonde launchings. Most of the observations are conducted during non-rainy days except two during 01:00–02:00 IST on 18 August 2011 and 14:00–20:00 IST on 21 August 2012, with total rainfall about 47 and 46 mm, respectively. In total 764 profiles of temperature, pressure, relative humidity (RH), and horizontal wind are obtained from the 34 campaigns. These data are collected using "Meisei RD-06G" radiosonde observations sampled at 10 m (sampled at 2 s intervals) under the TTD campaigns (Ratnam et al., 2014). The observed dataset is gridded uniformly to 30 m altitude resolution so as to remove any outliers arising from random motions of the radiosonde, if any, or very high frequency fluctuations but at the same time to retain the ABL signature. Note that gridding these data to coarser resolution (e.g., 100 m) smooths out the ABL detection, especially the SBL, which lies generally below 0.5 km above ground level. Quality checks are then applied to remove any further outliers arising due to various reasons to ensure high quality in the data (Mehta et al., 2011).

2.2 Infrared brightness temperature (TBB) data

In order to understand the role of clouds, especially low-level clouds occurring around the ABL, the cloud top temperature (CTH) is estimated using TBB obtained from the Climate Prediction Centre, NOAA, available at a time resolution of 1 h and spatial resolution of $0.03^\circ \times 0.03^\circ$. These are globally merged, full-resolution ($\sim$4 km) IR data formed from the $\sim$11 micron IR channels aboard the GMS-5, GOES-8, Goes-10, Meteosat-7, and Meteosat-5 geostationary satellites. The data have been corrected for zenith angle dependence to reduce discontinuities between adjacent geostationary satellites. For this study, we averaged the TBB data into 0.25° latitude $\times$ 0.25° longitude grid around Gadanki and collected for every 3 h during each campaign. The cloud top height is obtained from the radiosonde temperature profiles as the altitude corresponding to averaged TBB.

2.3 Method of analysis

Altitude profiles of temperature variables and moisture variables obtained from the radiosonde observations are used to estimate the ABL height based on different methods. Seven different methods, two using the temperature profile, three using the moisture profile, and two a combination of temperature and moisture profiles, are adopted to estimate the ABL height in each sounding. The temperature variables are dry air temperature (T) and potential temperature (θ) and the moisture variables are RH, specific humidity (q), and water vapor pressure (P_w). The combination of both temperature and moisture variables is the virtual potential temperature (θ_v) and radio refractivity (N). The ABL height is generally identified as the location of (1) the maximum vertical gradient of one of the variables T, θ, or θ_v or (2) the minimum vertical gradient of one of the variables RH, q, P_w, or N (Sokolovskiy et al., 2006; Basha and Ratnam, 2009; Seidel et al., 2010; Chan and Wood, 2013) below 3.5 km above the surface. We limited the altitude region to 3.5 km, following Chan and Wood (2013) who used GPS radio occultation refractivity data to study the seasonal cycle of the ABL over the globe. The upper limit 3.5 km is selected in order to avoid midlevel inversions, if any. When more than one peak in the gradient occurs below 3.5 km, the lowest peak with a value greater than 80 % of the main peak is considered as the ABL top. As suggested by Ao et al. (2012), the gradient-based ABL definitions are most meaningful when they are large in magnitude relative to the average gradient. They defined the "sharpness parameter" as $X'_S = |-X'_{\min \text{ or } \max}/X'_{RMS}|$, where X is moisture or temperature variables and X'_{RMS} is the root mean square (RMS) value of X' over the altitude range 0–3.5 km. If $X'_S \geq 1.25$ it is considered that ABL is well defined. In the case of SBL the gradient at the top of the RL is much stronger than that of the gradient at the top of the SBL. The SBL is generally identified using surface-based inversion (SBI) methods (Seidel et al., 2010). At the SBL, where temperature increases sharply, the temperature gradient shows a maximum value immediately just above the surface, but not at the actual level where the temperature reverses from the positive to negative gradient. In the present study, the SBL is identified as the level of maximum temperature below 0.9 km. The upper limit for the SBL height identification is based on Kumar et al. (2012), who observed the maximum wind speed (sporadic region) deep enough up to $\sim$0.9 km. The method to obtain the RL is similar to that of the CBL.

Following the above criteria, we have obtained the CBL, SBL, and RL heights during each campaign listed in Table 1. Out of 764 profiles, 17 profiles are rejected due to bad quality data. In the nighttime two types of profiles are observed: one in which the SBL is present and the other in which the SBL is not present. The profiles for which the SBL is defined are further subdivided into two cases: (i) with the RL not defined and (ii) with the RL defined. As the observations are at 3 h intervals, actual changes happening during the morning transition (MT) and evening transitions (ET) during the course of diurnal cycle might not have been captured. Sandeep et al. (2015) have made a comprehensive study on the transitory nature of the ABL during ET over Gadanki. They found that the transition follows a top-to-bottom evolution. Note that the mean sunrise time is about 05:45 IST (06:30 IST) while sunset time is about 18:30 IST (17:45 IST) during the summer (winter) over Gadanki.

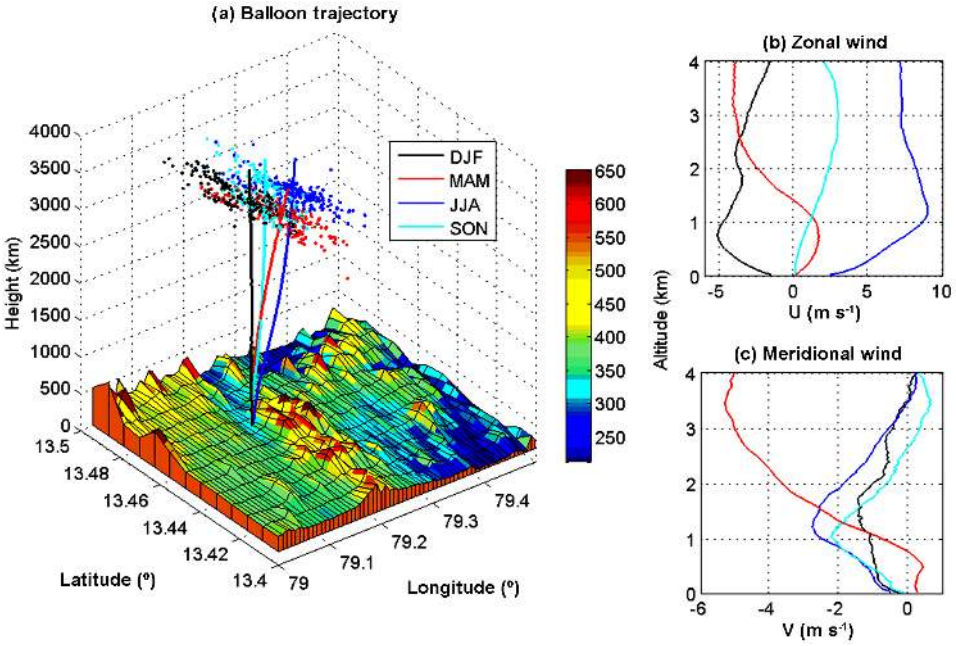

Figure 1. (a) Topographical features surrounding the location of radiosonde launch site, Gadanki (13.45° N, 79.2° E), a tropical station in India, along with profiles of seasonal mean trajectories (thick lines) from the surface to 4 km and the locations of the balloon reaching at altitude 4 km (dots) during different seasons. The mean **(b)** zonal wind and **(c)** meridional winds for different seasons observed during the period December 2010–March 2014. Global 30 arcsec gridded topography data are provided by the National Centre for Environmental Information, USA.

The lifting condensation level (LCL) is defined as the height at which an unsaturated air parcel becomes saturated (RH > 100 %) when it is cooled by dry adiabatic lifting (Wallace and Hobbs, 2006). It provides an empirical estimate of the cloud base height. The temperature (T_L) and height (Z_L) of the LCL are obtained using the following equations (Bolton, 1980):

$$T_L = \frac{2840}{3.5\ln(T_{30\,m}) - \ln(P_{w\,30\,m}) - 4.805} + 55, \quad (1)$$

$$Z_L = -(T_L - T_{30\,m})/\tau_d, \quad (2)$$

where $T_{30\,m}$ and $P_{w\,30\,m}$ are temperature and water vapor pressure at 30 m height, respectively, and τ_d is dry adiabatic lapse rate.

3 Results

3.1 Topography, balloon trajectory, and mean wind pattern over Gadanki

Figure 1a shows the seasonal mean trajectories of balloon below 4 km and locations of balloons at 4 km during different seasons launched over Gadanki for the period December 2010–March 2014. Gadanki is surrounded by hills of maximum height of 500–600 m above the mean sea level. Towards the west of Gadanki is the chain of the Nallamala Hills with height about 800–1000 m and the eastern side of it is flanked by Bay of Bengal. Note that Gadanki is a far inland station (∼ 120 km away from the Bay of Bengal coast) and hence does not have any local effect due to the sea. The balloon generally drifted about 0.1 and 0.2° in latitude and longitude, respectively, below 4 km. It can be seen that the balloon ascended almost vertically and drifted towards the southwest direction during the winter season (DJF; December–January–February) while during summer monsoon season (JJA; June–July–August) it drifted mostly towards the southeast. During pre-monsoon (MAM; March–April–May) the balloon ascended almost vertically up to 1 km and drifted southward to above 4 km. In the post-monsoon months (SON; September–October–November) it ascended almost vertically up to 2–3 km and changed direction towards the southeast.

Figure 1b–c show the seasonal mean zonal (U) and meridional (V) winds, respectively, obtained using averaging horizontal wind data observed during the period December 2010–March 2014. Within the ABL, it can be seen that the zonal winds are mostly easterly during the winter and pre-monsoon and westerly during the summer monsoon and post-monsoon and the meridional winds remain southerly throughout the year. During the summer monsoon season, low level westerly jet (LLJ) core of 10 m s^{-1} at 1 km is clearly evident.

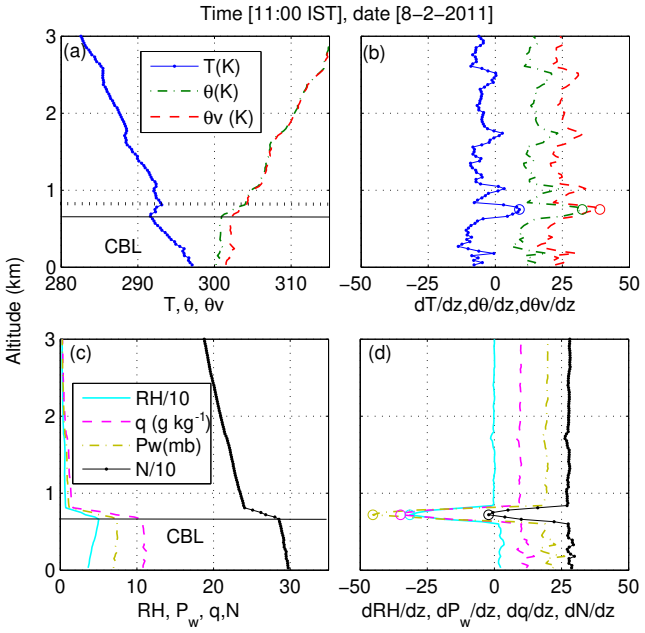

Figure 2. Typical profiles of **(a)** temperature (T), potential temperature (θ), and virtual potential temperature (θ_v) as well as **(c)** relative humidity (RH), specific humidity (q), water vapor pressure (P_w), and radio refractivity (N), showing convective boundary layer (CBL) using GPS radiosonde observation at 11:00 IST on 8 February 2011 over Gadanki (13.45° N, 79.2° E). **(b)** and **(d)** show the gradient profiles corresponding to **(a)** and **(c)**, respectively. Solid horizontal lines in **(a)** and **(c)** indicate the base of the inversion layer. Dotted line in **(a)** indicates the top of the inversion. Open circles in figures **(b)** and **(d)** denote the CBL heights above ground level.

3.2 Identification of the ABL (CBL and SBL) from temperature and moisture profiles

Figure 2 shows the typical profiles of the temperature variables T, θ, and θ_v and the moisture variables RH, q, P_w, and N observed at 11:00 IST on 8 February 2011 to identify the CBL. Note that these profiles are observed in clear sky conditions (TBB ∼ 295 K). It can be seen that the CBL is capped by the inversion layer of thickness 0.150 km, where a sharp increase in temperature and a sharp decrease in the moisture variables occur. The base of the entrainment zone is at 0.69 km above the ground level, which is defined as the top of the CBL. Within the CBL, θ, θ_v, q, and P_w are almost constant, with altitude signifying that the air is mixed or having a tendency towards vertical mixing due to the action of the turbulence, a characteristic of the "mixing layer" (Seibert et al., 2000). Above the CBL and within the entrainment zone T, θ, and θ_v increase sharply by about 1.5, 3.0, and 2.0 K, respectively, and moisture variables (RH, q, P_w, and N) decrease sharply by about six times. At the top of the entrainment zone, θ_v coincides with θ as water vapor concentration becomes very small. These sharp changes at the CBL top are easily captured by the gradient of the temperature and moisture variables as shown in Fig. 2b and d, respectively. Both the maximum gradient of the temperature variables and the minimum gradient of the moisture variables identify the CBL height quite well.

As mentioned earlier, after sunset (in the nighttime) the identification of the SBL is not as easy as the identification of the CBL, mainly because of the absence or delay in the formation of the surface inversion due to weak surface cooling. Therefore, whenever the SBL is not present the ABL is represented as the RL. Typical examples of identification of the SBL are shown in Fig. 3a–l for three different types of nighttime temperature (T, θ, and θ_v) and moisture (RH, q, P_w, and N) profiles and their corresponding gradient profiles, indicating the presence of the SBL but not the RL, both the SBL and the RL, and not the SBL but the RL, respectively. The temperature and moisture profiles and their corresponding gradient profiles observed at 02:00 IST on 9 February 2011 show the evolution of the SBL only but not the RL (Fig. 3a–d). The gradients of temperature profiles and moisture profiles shown in Fig. 3b, d are offset by a scale of 10. These profiles are observed during fair weather conditions (TBB ∼ 295 K). The top of the SBL identified based on the SBI in T is indicated as a horizontal dashed line in Fig. 3a. The SBL is identified at 0.39 km above ground level. Within the SBL both θ and θ_v increase steeply. The temperature gradient profiles show a maximum gradient at the surface which steeply decreases within the SBL (Fig. 3b). The moisture profiles (Fig. 3c) also show a steep decrease within the SBL. However, their gradients (Fig. 3d) show a negative peak at 0.18 km observed at a lower height when compared to the top of the SBL. The negative gradient peaks in the moisture variables are denoted as open circles. The sharp changes in the moisture variables in the SBL are indicative of inversion forming adjacent to the surface similar to the formation of entrainment zone aloft in the development of the CBL. Thus, one can also identify the height of the SBL based on moisture gradient peaks (especially when temperature observation is not available) near the surface when the RL is absent. However, it becomes difficult when the gradient aloft is strong, as will be seen in the later examples.

A similar feature can be noted in the case of the SBL forming beneath the RL as identified using temperature and moisture variables, shown in Fig. 3e–h, observed at 02:00 IST on 19 December 2013. These profiles are observed under deep convective conditions with the TBB value about 262.3 K and corresponding CTH is 6.67 km. In this case, the SBL based on the SBI is identified at 0.21 km above the ground level (Fig. 3e). The temperature variables increase and moisture variables decrease in the SBL (Fig. 3e and g), but not as steep as the previous profiles shown in Fig. 3a and c, respectively. The gradient method identifies the RL top at 1.35 km denoted by open circles as shown in Fig. 3f and h. The RL has similar features as the CBL mentioned in Fig. 2. One can observe a weak gradient in the moisture variables (Fig. 3h) at 0.30 km. It can be assigned as the top of the SBL defined using the gra-

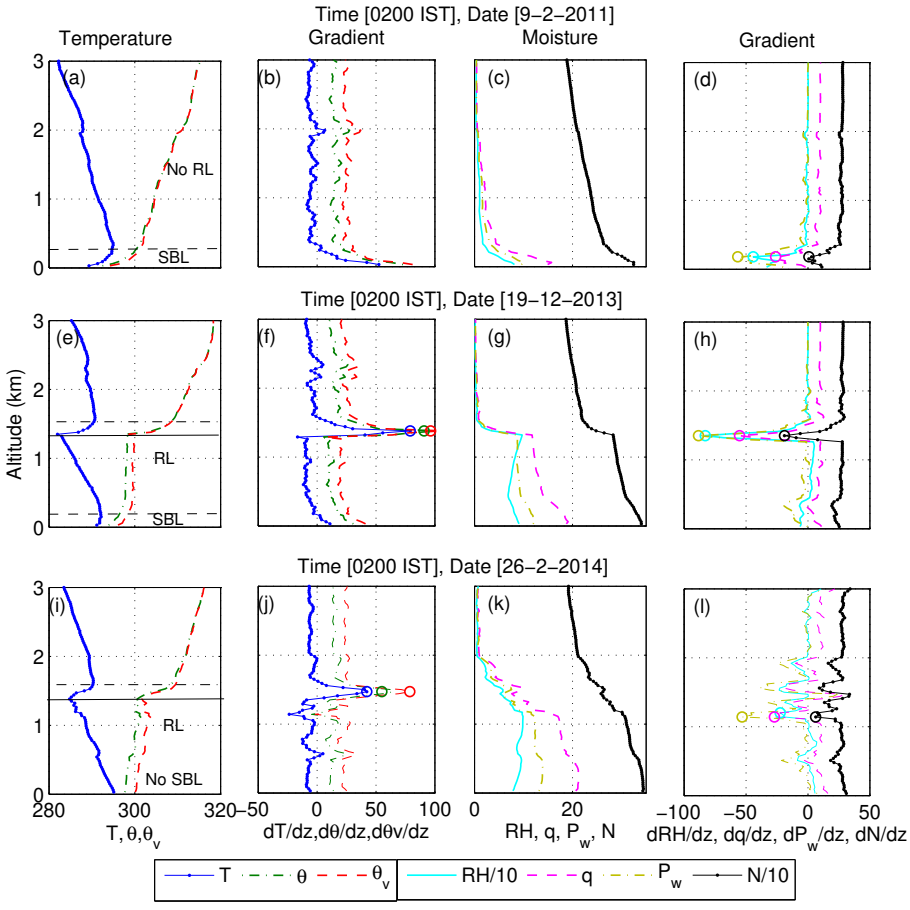

Figure 3. Same as Fig. 2 but for nighttime profiles observed at 02:00 IST, indicating **(a)** the stable boundary layer (SBL) but not the residual layer (RL) observed on 9 February 2011, **(b)** both the SBL and the RL observed on 19 December 2013, and **(c)** the RL but not the SBL observed on 26 February 2014. The horizontal dashed lines denote the surface-based inversion in the temperature profile and open circles denote maximum gradients in temperature variables or minimum gradients in the moisture variables. Horizontal dash-dotted lines indicate capping inversion layer.

dient method in the moisture, which is slightly higher than the SBL defined using SBI. However, the SBL identification from the negative gradient peak in the moisture profiles becomes difficult when strong RL is present, as can be noticed from the next example.

Unlike the above-mentioned cases, an example indicating no SBL formation beneath the RL in both temperature and moisture profiles observed at 02:00 IST on 26 February 2014 is shown Fig. 3i–l. In this case, the feature of the RL is similar to that shown in Fig. 2 for the CBL and that shown in Fig. 3e–h for the RL. Like CBL, it also starts from the surface. By definition the RL is the layer observed above the SBL and hence not considered as the ABL. However, if the SBL is absent as in this case, the RL will be above the surface and it is nothing but nighttime ABL. In a study more similar in concept to ours, Liu and Liang (2010) pointed that such cases are generally identified with near-neutral conditions in the surface layer, which they assigned as the neutral RL (NRL) that starts from the ground surface. However, in our study, we refer to it simply as the RL. Using gradient method, the top of the RL is identified at 1.47 km from the temperature variables and at 1.14 km from the moisture variables. The moisture profiles and its corresponding gradients are disturbed for about 1.0 km above the RL. Unlike the previous examples, the moisture profiles in this case do not sharply decrease. The TBB at 02:00 IST on 26 February 2014 is 289.4 K and the corresponding CTH is 0.81 km, indicating the presence of the low level fair weather clouds. The RL height difference observed using temperature and moisture variables is difficult to explain, but it seems affected by the presence of clouds. The surface moisture is very small and the LCL observed at about 0.6 km indicates that a shallow layer cloud of thickness about 0.2 km decoupled from the surface (Garratt, 1992). The absence of the SBL indicates lack of sufficient surface cooling, which could be due to presence of clouds above radiatively warming the surface. It should be noted that there is a weak gradient present in both temperature and moisture variables at 0.51 km, which is very

small when compared to the gradient at the RL. Comparing the moisture gradients below the RL top shown in Fig. 3l with that presented in Fig. 3h, it is inferred that the gradient below the RL may not always be due to the surface cooling. Hence, identifying the SBL using moisture variables based on the gradient method needs caution. Thus, in the present study, we preferred the identification of the SBL based on the SBI only.

3.3 Typical diurnal variation of the ABL

From the previous typical examples presented for the particular times, it is observed that the ABL identified using the temperature and moisture variables independently agree fairly well. Thus, any one temperature variable and any one moisture variable are sufficient to document the ABL variation. It is also observed that the ABL heights are well identified during different cloudy conditions. Thus, hereafter we only examine T, θ_v, q, and N for the rest analysis. θ is related to θ_v and RH and P_w are related to q; thus θ, RH and P_w are dropped from further analysis. The typical examples of the 3-hourly variations of the CBL, SBL, RL, CTH, and the LCL observed over 3 days are shown in Fig. 4a–d for the four different types of diurnal variation indicating formations of well-defined SBL, delayed SBL, no SBL, and the intermittent SBL, respectively. Figure 4a–d also show four different cloud conditions occurring around the ABL, far above (deep convection) the ABL, below the ABL, and just above the ABL, respectively. The first three (Fig. 4a–c) panels show the complete 3-day observations for which the typical examples of the particular times have been described earlier in Figs. 2 and 3. Note that the diurnal variation of the CBL and RL is identified based on T, θ_v, q, and N variables, while the SBL is identified using T variable only.

Figure 4a shows the perfect diurnal evolution of the ABL for all 3 days observed during 8–11 February 2012 (see Supplement Fig. S1, which depicts the corresponding vertical profiles T, q, and N along with the TBB and CTH). The CBL height just before noon (11:00 IST) is at height 0.69 km on the first day, which further grows to height 1.2 km during afternoon (14:00 IST) due to the maximum surface heating and remains at the same height until evening (17:00 IST) just before the sunset (18:16 IST). During this time ET takes place and the development of the SBL started and observed at height 0.48 km on 20:00 IST, which descends slowly during its nighttime evolution to the height 0.15 km at 08:00 IST on the second day. Due to development of convective turbulence after the sunrise (06:39 IST), the SBL is in the stage of the disappearance after 08:00 IST, probably indicating the activity of MT. During the second and third days, the evolutionary feature of the CBL and SBL are similar to that on the first day; however, they show large day-to-day variability. The CBL was not identified either by using moisture or by temperature variables at 11:00 IST on the second day (Fig. S1 in the Supplement). Either clear sky conditions or the CTH below the CBL are observed during the first and third days (TBB $\sim$ 295 K). During the second day, TBB reduced by about 10 K, indicating presence of the low level clouds with CTH at 2.5 km. The diurnal variation of the ABL shows the CBL at the same height using all the variables on the first day, but they differ on the second and third days. The CBL height identified from the minimum gradients of q and N are exactly the same, indicating the dominance of the moisture part in the N when compared to T. Similarly, both T and θ_v identify the same heights of the CBL and RL, indicating dominance of the temperature in θ_v when compared to the moisture. The RL is not observed on the first night; it appears on the second and third nights, which generally decreases in the course of the night.

A similar example of typical 3-day diurnal variation of the ABL identified using T, θ_v, q, and N profiles in which delay in the SBL formation is observed during 18–21 December 2013 is shown in Fig. 4b (see corresponding vertical profiles in Fig. S2 in the Supplement). During this case during deep convection events are observed. In this case, the CBL height just before noon is observed at 1.59 km and remains at about the same height until evening. After the sunset, the CBL did not collapse. The formation of the SBL begins at midnight, indicating delay in ET process. Thus, the ABL heights observed at 20:00 and 23:00 IST are the RL top heights. The SBL appears at height 0.18 km after midnight (02:00 IST) and remains at about the same height until morning (08:00 IST) on the second day. On the second day, the CBL reappears again at 1.35 km before noon, which became maximum (1.83 km) afternoon and steadily decreases to 1.53 km at 20:00 IST. The ET process again delayed and the SBL did not form until just before the midnight on the second day. On the third day, the CBL varies in similar fashion as on the second day but this time the ET process was not delayed and the SBL formed on 20:00 IST. On the third night the SBL was detected at a height about 0.45 km. Note that both the temperature and moisture profiles show wave-like features during 20:00–08:00 IST on the third night could be either due to strong horizontal advection or due to gravity wave propagation (Fig. S2 in the Supplement), which will be examined in a separate study. The RL during all 3 days remain about the same height in contrast to the previous example in which it decreases as the night progresses.

The TBB ranges from 285 to 218 K, corresponding to CTH of about 2.46–11.6 km, respectively. From the first day (18 December 2013) to the evening of the third day (20 December 2013), deep convection prevails, with the CTH above 6 km except a few occasions when it lowers down to about 3.0–4.0 km. From midnight of the third day CTH was observed below 3.0 km, during which T, q, and N were observed to be disturbed (Fig. S2 in the Supplement). The delay in the ET processes seems related to the warming caused by cloudy skies, which might have resulted in a delay of the surface cooling during the early part of the first and second nights. However, it must be noted that the presence of clouds

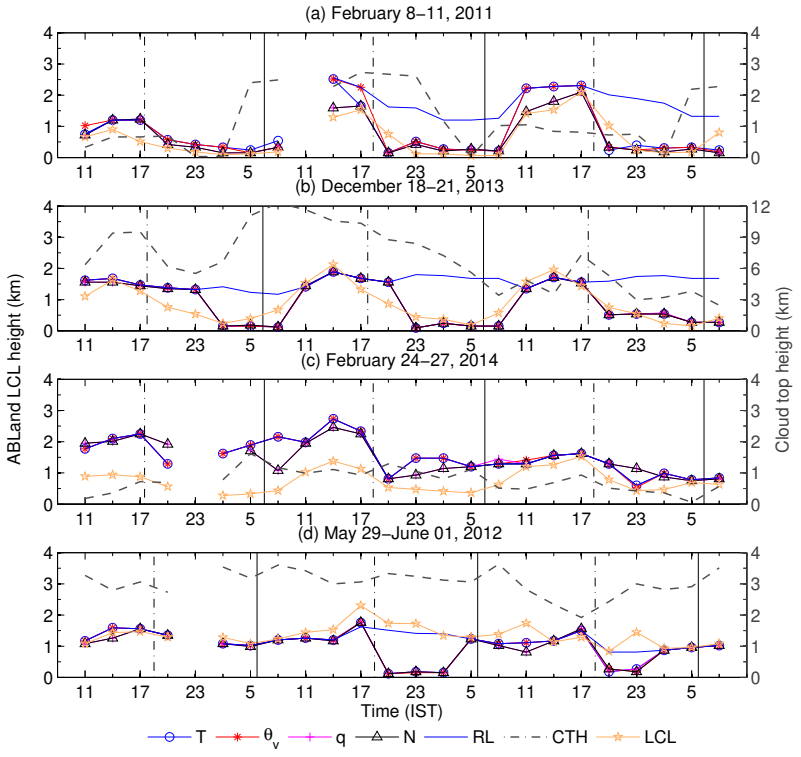

Figure 4. Diurnal variability of the ABL (CBL, SBL, and RL) height obtained from the variables T, θ_v, q, and N during **(a)** 8–11 February 2011, **(b)** 18–21 December 2013, **(c)** 18–21 February 2013, and **(d)** 29 May–1 June 2012. Thick dashed lines indicate the cloud top height (CTH). Yellow star lines indicate the lifting condensation level (LCL). Vertical dashed and solid bars indicate sunset and sunrise times, respectively.

could be one possible reason as there are occasions when the SBL forms even in the presence of clouds. Hence, the delay in the ET process cannot be entirely explained by the longwave effect. It can be seen that, during the deep convection conditions, the ABL identified using different moisture and temperature variables is the same.

Another typical 3-day variation of the ABL, where the SBL is not formed throughout the observation period and when clouds lying below the ABL as shown in Fig. 4c, is observed during 24–27 February 2014 (see Fig. S3 in the Supplement for the vertical profiles). Thus, during nighttime, the RL is only defined which is above the surface and considered as nighttime ABL. None of the temperature profiles show the evolution of the SBI (Fig. S3 in the Supplement). The ABL is at about 2.0 km (11:00–17:00 IST), which descends down to height 1.14 km (20:00 IST) and to 0.66 km (23:00 IST) on the first day. The CTH indicates the presence of low level clouds at about 1.0–1.5 km between the evening of the first day and early morning of the second day. An example of the typical 3-day variation of the ABL, where SBL is defined intermittently and when clouds lying above the ABL are shown in Fig. 4d observed during 29 May–1 June 2012 (see Fig. S4 in the Supplement for vertical profiles). By intermittent we mean the SBL is defined a few times but not the whole night. In this case, the TBB ranges from 290 to 276 K, corresponding to the CTH from about 1.96 to 3.60 km. The CTH is always above the ABL. On the first day, the SBL does not form and the ABL is almost at about the same height until the evening of the second day. On the second and third nights the SBL formed sometimes. In all the above cases, the SBL has either decreased after midnight or remained constant. These two types of the SBL are somewhat equivalent in types reported by Kumar et al. (2012). During clear sky conditions, the constant and decreasing SBL heights after midnight are generally accompanied by steady and unsteady winds (Kumar et al., 2012).

The typical diurnal variations of the LCL for the four different cases of clouds are shown in Fig. 4a–d. In general, it is observed that the LCL forms below the ABL (CBL + RL) except for a few cases. During 8–11 February 2011, the LCL occurs just above the CBL (Fig. 4a) but below the RL. During the second day when the CTH occurs at 2.4 km, the LCL also forms near to it. However, the LCL is also higher than the CBL on the first day and the third day, when the CTH is very low. It indicates that the LCL and CTH are not always related. In the case of deep convention conditions during 18–21 December 2013, the LCL shows nice diurnal cycle similar to the ABL (CBL + SBL) (Fig. 4b). During 24–

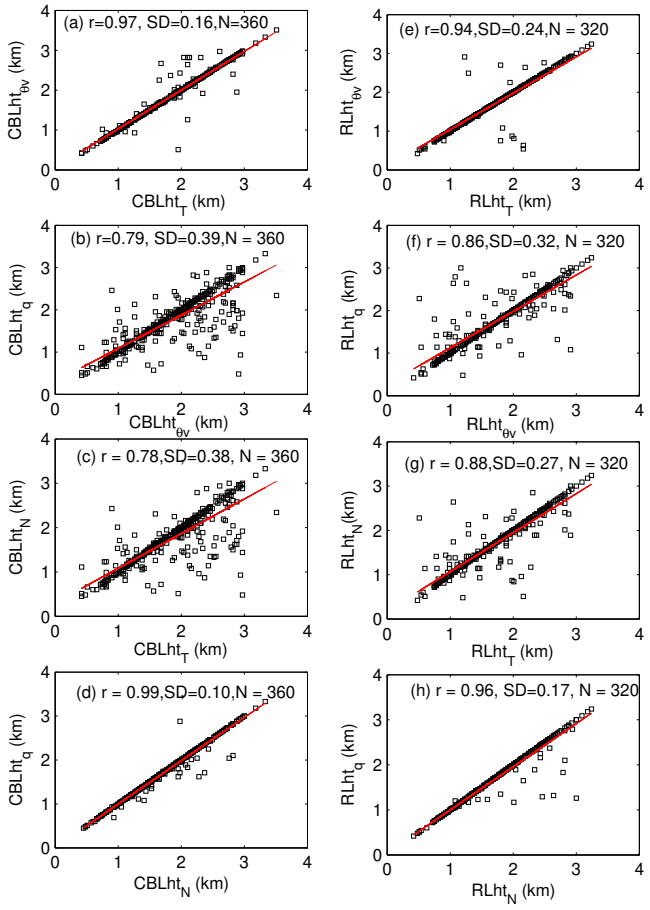

Figure 5. Scatter plot between the CBL heights obtained using **(a)** T and θ_v, **(b)** θ_v and q, **(c)** T and N, and **(d)** N and q. **(e–h)** are same as **(a–d)** but the RL heights.

27 February 2014, the case when the CTH is occurring below the ABL, the LCL also occurs below the ABL and at or around the CTH (Fig. 4c). During 29 May–1 June 2012, when the CTH is well above the ABL, the LCL remains almost constant and varies in a similar way as the CBL and RL (Fig. 4d). From these typical cases, it appears that the ABL and the LCL are sometimes closely related and sometimes randomly. A detail comparison of the LCL with different ABL regimes is presented in the later section.

3.4 Correlation analysis

The typical examples of the SBL, CBL, and RL identification shown in previous section reveal that the different methods agree well except in a few cases. In order to see the overall correlation of the CBL and RL heights detected from T, θ_v, q, and N, a statistical comparison between them has been made as shown in Fig. 5. The total number of observations available during daytime (08:00–17:00 IST) is 379. Out of these, the CBL is defined in 360 profiles (see Table 1), the CBL is not defined in 18 profiles, and 1 profile is rejected due to bad quality data. The total number of observations available during nighttime (20:00–05:00 IST) is 385. Out of these, the RL is defined in 320 profiles as listed in Table 1, the RL is not defined in 49 profiles, and 16 profiles are rejected due to bad quality data during the quality check process. Figure 5a–d show the scatter plots of the CBL heights obtained using four different methods.

The correlation between the CBL heights obtained from T and θ_v ($r = 0.97$) (Fig. 5a) and q and N ($r = 0.99$) (Fig. 5d) are found to be excellent, which have a standard deviation (SD) of 0.16 and 0.10 km, respectively, suggesting that it can be determined using either of the methods. However, the correlations between the CBL heights obtained from θ_v and q ($r = 0.79$) (Fig. 5b) and T and N ($r = 0.78$) (Fig. 5c), though agreeing well, have a large SD of about 0.39 and 0.38 km, respectively. Several times, the CBL height determined from temperature variables is higher than that one obtained from the moisture variables. There could be various reasons for this disparity, however, whenever the temperature and moisture gradients are sharper or having significant gradients (Basha and Ratnam, 2009), both methods define unique height, but differences occur when they are not so sharp. Seidel et al. (2010) observed no correlation between the ABL heights obtained using T (elevated inversion) and the rest of the methods (θ_v, q, N). Surprisingly, they observed good correlation between $\theta$and moisture variables (q, RH, N) but no correlation with T. In fact, θ mostly depends upon the T variation, so one would expect a good correlation between them as observed in our case.

Figure 5e–h show the scatter plots of the RL heights obtained using four different methods. Similar to the CBL heights, the RL heights also show excellent correlation between T and θ_v ($r = 0.94$) (Fig. 5e) and q and N ($r = 0.96$) (Fig. 5h), with SD of about 0.24 and 0.17 km, respectively. The correlation between RL heights obtained from θ_v and q ($r = 0.86$) (Fig. 5f) and T and N ($r = 0.88$) (Fig. 5g) with SD about 0.32 and 0.27 km, respectively, is comparatively better than the CBL heights. However, unlike the CBL heights, the RL heights estimated using different methods scatter uniformly about the linear fit, indicating that sometimes the RL heights obtained using temperature variables are higher than that of moisture variables and vice versa. As we have observed excellent correlation between different methods, hereafter the rest of the results will be presented using T variable only, because both the SBL and CBL can be easily estimated using this variable.

3.5 Statistics of the SBL, CBL, and RL heights

Before proceeding to the diurnal variation of the ABL, we first document the occurrence statistics of the SBL, CBL, and RL and the general nature of their diurnal cycle as shown in Fig. 6. The occurrences of the SBL, CBL, and RL and the occurrences of the SBL during different seasons are shown in Fig. 6a and b, respectively. The SBL forms mainly dur-

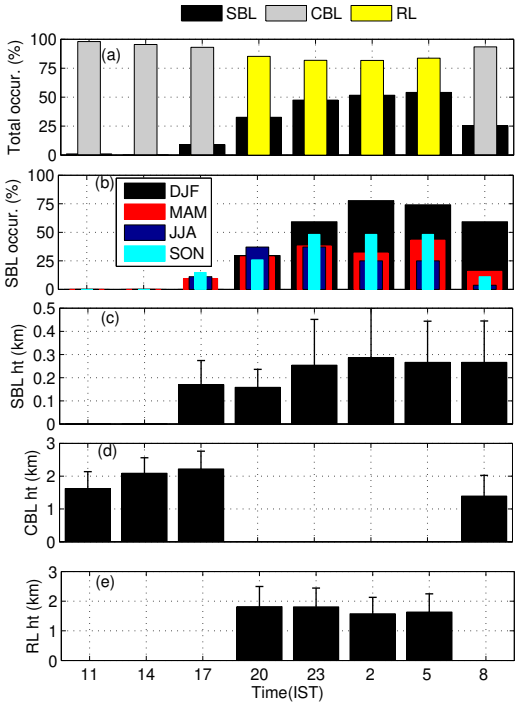

Figure 6. (a) Total percentage occurrence of the SBL, CBL, and RL heights; **(b)** percentage occurrence of the SBL during different seasons. Mean and standard deviations of **(c)** the SBL height observed at 3 h interval between 17:00 and 08:00 IST, **(d)** the CBL observed at 3 h interval between 08:00 and 17:00 IST, and **(e)** the RL observed at 3 h interval between 20:00 and 23:00 IST. These statistics are obtained using *T* variables.

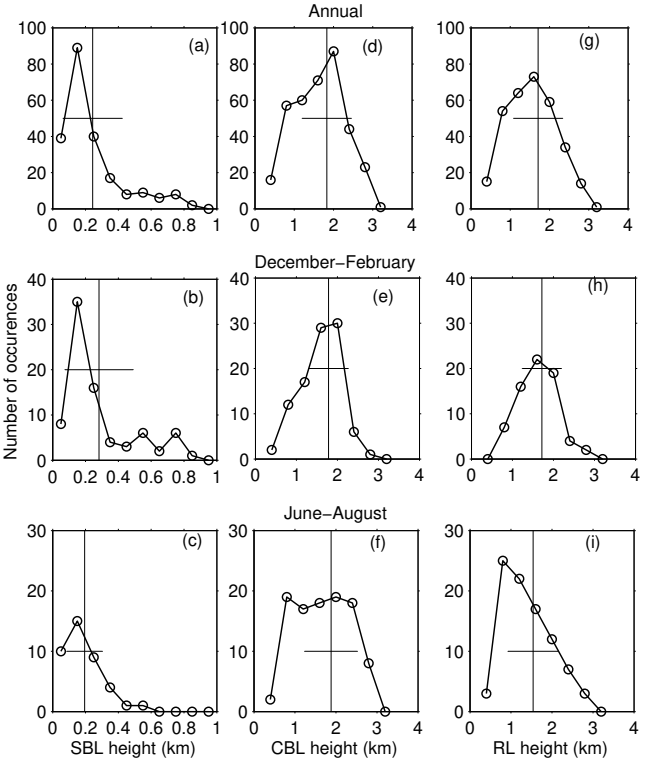

Figure 7. Probability distribution of 3-hourly (left column panels) SBL height with 0.1 km interval obtained for **(a)** annual, **(b)** winter, and **(c)** summer from the data observed during December 2010–March 2014. **(d–e)** same as **(a–c)** but for the CBL height; **(f–h)** are same as **(a–c)** but for the RL height with 0.4 km interval. The points at which the vertical line intersects the *x* axis represents their mean heights while the length of the horizontal bar represents the corresponding standard deviations.

ing nighttime, except a few times during the early evening (17:00 IST) and the late morning (08:00 IST). The SBL occurrence dominates at nighttime (23:00–05:00 IST) with occurrence about 50 %. At 20:00 IST, occurrence of the SBL is only 33 %, indicating a delay in surface cooling about 17 % of the time. Over Gadanki, the occurrence of the SBL is less than the occurrence over land in the midlatitude (North America and European regions) (Liu and Liang, 2010). The SBL observed at 08:00 IST for about 25 % of the time, indicating the dominance of the surface cooling even after (generally 2 h after) the sunrise. As surface cooling starts well before (generally 2 h before) the sunset, sometimes (about 9 %) SBL also forms at 17:00 IST. In general, the SBL occurs more frequently during the winter when compared to the summer monsoon season. Liu and Liang (2010) also observed occurrences of the SBL a few times during midday. However, we have not observed such occurrence over Gadanki. It is interesting to note that the SBL at 08:00 IST mostly formed during the winter months. During winter, when sunrise is at ∼ 06:30 IST, surface cooling may remain strong until 08:00 IST on some days, leading to the formation of the SBL. Whereas during the summer monsoon season with sunrise at about 05:45 IST, surface cooling may not last until 08:00 IST, leading to very few occurrences of the SBL at 08:00 IST. The CBL and RL occurrences dominate and are evenly distributed at 3 h intervals during daytime (08:00–17:00 IST) and nighttime (20:00–05:00 IST), respectively. In contrast to Liu and Liang (2010) we observed the uniform occurrence of the CBL at 3 h intervals during daytime.

Figure 6c–e show the mean height of the SBL, CBL, and RL along with their respective SDs between 11:00 and 08:00 IST. The mean SBL height varies between 0.16 ± 0.07 km at 20:00 IST and 0.29 ± 0.21 km at 20:00 IST. The overall mean SBL is below 0.3 km above the surface consistent with the literature (Stull, 1998). After the sunrise, the CBL starts to form which lies between 1.4 ± 0.62 km at 08:00 IST and $\sim 2.0 \pm 0.5$ km at 14:00–17:00 IST (Fig. 6b). Overall the mean CBL height is well below the 3.0 km above the surface consistent with the available literature (Stull, 1988; Garratt, 1994). The daytime CBL remains prevalent as part of the RL during nighttime, which slightly falls to 1.8 ± 0.67 km at 20:00 IST and becomes minimum 1.6 ± 0.55 km at 02:00 IST (Fig. 6c).

We have examined the probability distributions in order to find out the most probable height at which the SBL, CBL, and RL occur in winter season, summer monsoon season, and the entire year as shown in Fig. 7. The SBL height distributions show a clear peak at 0.15 km during both summer and winter seasons as well as in the annual mean (Figs. 7a–f). The peak distributions and mean along with SD of the SBL indicate that the SBL heights are within 0.30 km, as consistent with the available literature, except a few times when SBL forms above it. The mean SBL height shows a clear seasonal variation with lower height during the summer monsoon season than the winter season. Figure 7d–f show the CBL height, which has clear peaks at about 2.0 km in the annual and winter season closely coinciding with the mean CBL. During the summer season, the CBL height distribution has a broad peak between 0.8 and 2.4 km, and the mean CBL height is slightly higher than that during the winter season. A clear seasonal variation is also observed in the mean CBL height. It indicates that the CBL heights are highly variable during summer monsoon season when compared to winter season. The RL height distribution is similar to that of the CBL height distribution in the annual and winter, which peaks at a relatively lower height $\sim$ 1.8 km (Fig. 7g–h). During the summer monsoon season, the RL height distribution shows a peak at 0.8 km in contrast to the CBL distribution. Liu and Liang (2010) have also observed similar distributions as reported in this study.

The distributions of the SBL, CBL, and RL mentioned above for the annual, winter and summer monsoon are again reproduced in terms of the box plot as shown in Fig. 8a–c, respectively. The median values the SBL during the annual, winter, and summer monsoons remain same (Fig. 8a). There are a few outliers whose values are greater than 3 times the corresponding interquartile ranges for the annual and two different seasons. The SBL mostly lies below 0.65 km during the winter and 0.4 km during summer monsoon. The SBL is more variable during the winter than summer monsoon. As mentioned earlier, the CBL is higher and more variable during the summer monsoon than winter (Fig. 8b). Similarly, the RL is also more variable during the summer monsoon than winter (Fig. 8c). In contrast to the CBL, RL is lower during the summer monsoon when compared to the winter.

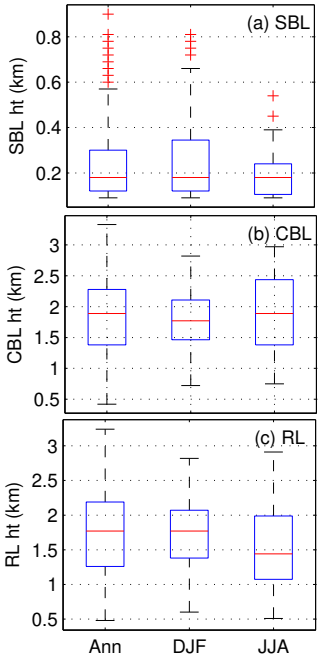

Figure 8. Box plot (representing median and interquartile ranges) of **(a)** SBL height, **(b)** CBL height, and **(c)** RL height for annual (Ann) winter (DJF) and summer monsoon (JJA) from the data observed during December 2010–March 2014.

3.6 Diurnal and seasonal variation of the ABL height

We have two combinations of the ABL variability: one is the CBL and the SBL denoted as the ABL_{CS} and another is the CBL and RL denoted as the ABL_{CR}. The diurnal variations of the ABL_{CS} height and ABL_{CR} height along with the surface temperature and the LCL height are shown in Fig. 9. The surface temperature is taken from the automatic weather station (AWS) observations over Gadanki. The diurnal variation of the ABL comprises of the CBL observed between 08:00 and 17:00 IST, the SBL between 17:00 and 08:00 IST, and the RL between 20:00 and 05:00 IST. As mentioned earlier, the mean CBL varies between $\sim$ 0.5 and 3.0 km and the mean SBL varies between $\sim$ 0.09 and 0.6 km. The mean diurnal variation of the CBL and the SBL (ABL_{CS} hereafter) shows that the CBL evolved slowly with time, attaining maximum height at 14:00 IST and either remaining constant or decreasing slowly until 17:00 IST and then collapsing to the SBL. The mean variation of the SBL over time is very small. It can be seen that the transition is more abrupt at 17:00 IST than the morning rise at 08:00 IST, which is consistent with earlier studies (e.g., Liu and Liang, 2010).

The variation of the CBL and RL (ABL_{CR} hereafter) over 3 days for all the campaigns is shown in Fig. 9b. Note that the CBL variation at 17:00 and 08:00 IST presented in Fig. 9a is relatively lower because the former also includes the SBL observations at 17:00 and 08:00 IST (see Fig. 6). It is interesting to note that the RL falls to a lower height during the most of the night and thus the ABL_{CR} shows a diurnal pattern with maximum height during 17:00 IST and minimum during early morning 08:00 IST. The observed maximum height of the CBL at 17:00 IST is found to be consistent with the general circulation model output (Medeiros et al., 2005). The RL height varies from $\sim$ 0.5 to $\sim$ 3.0 km. The RL is present throughout the night in most of the observations, which is sustained by the presence of the relatively warm air trapped between two stable layers: RL at the top and the SBL at the bottom. The trapped warm air slowly becomes cooler due to exchange of heat to the adjoining free atmosphere and gradu-

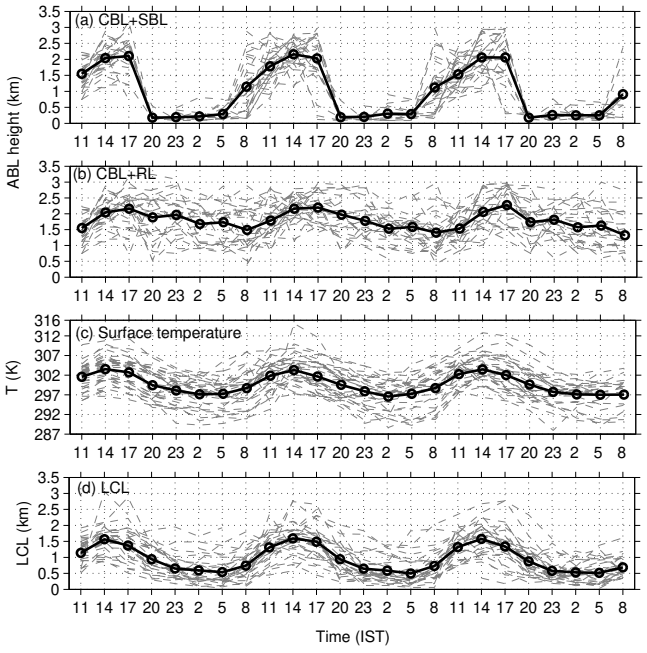

Figure 9. The 3-day diurnal variability of **(a)** the ABL (CBL + SBL) considering all the data observed for the CBL and SBL, **(b)** the CBL + RL considering all the data observed for the CBL and RL obtained using T variable, **(c)** the surface temperature, and **(d)** the LCL height observed during the period December 2010–March 2014.

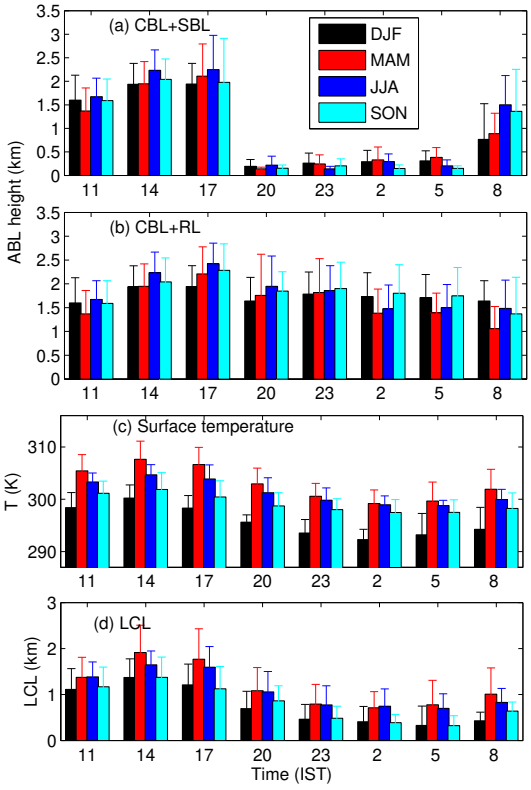

Figure 10. The diurnal variation of **(a)** the ABL_{CS} (CBL + SBL) height, **(b)** the ABL_{CR}(CBL + RL) height, **(c)** the surface temperature, and **(d)** the LCL height during different seasons.

ally intensifying SBL results in the descent of the RL during the course of the night, allowing the turbulence to decrease homogeneously in all directions.

The diurnal variation of the ABL_{CR} shows somewhat similar pattern as the surface temperature (Fig. 9c) and the LCL (Fig. 9d). Both the surface temperature and LCL become maximum at 14:00 IST and minimum at 02:00 IST. The diurnal pattern of the LCL height is similar to the pattern of the surface temperature. The mean LCL height is lower than the CBL and RL height. With higher surface temperature LCL is higher and vice versa.

Figure 10 shows the diurnal variation of the ABL height (obtained using T variable) and surface temperature during different seasons. We have considered those cases which show the diurnal pattern of the ABL, i.e., the formation of the CBL during daytime and SBL during nighttime as well as all those cases whenever SBL forms intermittently (excluding RL). As mentioned earlier, note that the occurrence frequency of the SBL just after the sunset is less than that of later periods at night. It means that the SBL has not always formed immediately after the sunset. Several times, formation of the SBL was delayed by 3–4 h after the sunset. Thus, we cannot expect a perfect diurnal variation in all the cases, especially when the SBL formation is delayed. In order to study the diurnal variation of the ABL, we have segregated all the CBL and SBL observed at 3 h intervals during the diurnal cycle in different seasons. Similarly, all the cases of the CBL and RL observed at 3 h intervals are also averaged into different seasons.

Figure 10a and b show the diurnal variation of the ABL_{CS} and ABL_{CR} during different seasons. In general, the CBL heights vary between 1.05 ± 0.46 and 2.25 ± 0.72 km, the SBL heights between 0.15 ± 0.05 and 0.33 ± 0.27 km, and the RL heights between 1.39 ± 0.41 and 1.94 ± 0.63 km. We have also obtained the diurnal variation of the surface temperature during different seasons as shown in Fig. 10c. In general, the diurnal patterns of the ABL_{CS} and ABL_{CR} during different seasons are same as the annual mean pattern shown in Fig. 9a and b, respectively. The diurnal variations of the ABL_{CS} show a seasonal pattern such that the CBL attains maximum height during the summer monsoon while the SBL during the winter to pre-monsoon. The amplitude of the diurnal evolution of the ABL_{CS} is stronger during pre-monsoon when compared to other seasons, i.e., maximum to minimum height variation is more during pre-monsoon when compared to other seasons. The SBL attains maximum height at 02:00 IST. Figure 10b shows that the ABL_{CR} height has a weak diurnal pattern during the winter when compared to summer. It is interesting to note that the CBL and RL heights reverse their seasonal pattern. The CBL height is higher dur-

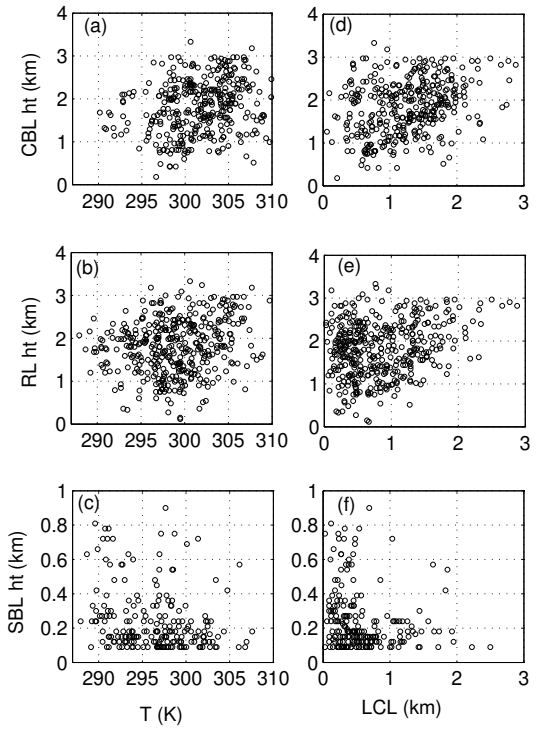

Figure 11. Scatter plot between the surface temperature and **(a)** CBL, **(b)** RL, and **(c)** SBL. **(d–f)** are the same as **(a–c)** but for the LCL.

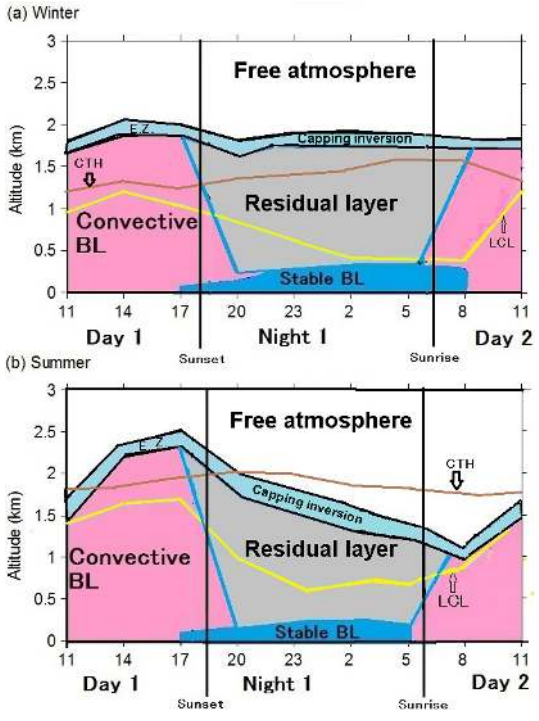

Figure 12. Schematic diagram of the vertical cross section of the mean ABL structure along with LCL and CTH during the **(a)** winter (DJF) and **(b)** summer monsoon (JJA) seasons over Gadanki. E.Z. indicates entrainment zone.

ing the summer and is lower during the winter in contrast to the RL height, which becomes higher during the winter and lower during the summer. In general, the CBL attains maximum height at 14:00–17:00 IST and minimum during 08:00–11:00 IST during all the seasons.

Figure 10c and d show the diurnal variation of the surface temperature and LCL during different seasons, respectively. Both the surface temperature and the LCL are the highest and lowest during pre-monsoon and winter, respectively. The highest amplitude of the diurnal variation of the ABL_{CR} can be attributed to the highest surface temperature during pre-monsoon. Similarly, the weak diurnal pattern of the ABL_{CR} can be attributed to the lowest surface temperature during the winter. In general, the LCL is lower than ABL_{CR} throughout the year. The difference between the LCL and CBL height is more during the winter and post-monsoon than pre-monsoon and summer monsoon.

As mentioned earlier, the diurnal evolution of the annual and seasonal mean pattern of the ABL is closely associated with the surface temperature. In order to see their 3-hourly relationships, we obtained the scatter plot of the CBL, RL, and SBL with the surface temperature as shown in Fig. 11a–c, respectively. Broadly, the scatter diagram indicates that the warmer the surface is, the higher the CBL and RL are and vice versa (Fig. 11a–b). However, these features are not always consistent and several times they occur randomly. In contrast to the CBL and RL, SBL is higher over the colder surface and vice versa, but these features are also not always consistent and several times they occur randomly (Fig. 11c). The corresponding 3-hourly relationship between the LCL and CBL, RL, and SBL is shown in Fig. 11d–f, respectively. The scatter plot between the CBL and LCL indicates that they occur randomly. The LCL generally occurs either below or at the CBL and RL except a few times when it occurs above the CBL and RL (Fig. 11d–f). The cases when the LCL occurs above the CBL or RL, clouds may not be generated by the processes driven by the ABL and can be formed due to large-scale dynamics (Anurose et al., 2016). We observed no relationship between the SBL and LCL (Fig. 11f). For the SBL case, as the vertical motion is inhibited, the relationship between the LCL and SBL is irrelevant (Anurose et al., 2016). Anurose et al. (2016) also studied the relationship between the CBL height and the LCL over the coastal station, Thiruvananthapuram (8.5° N, 76.9° E), they did not observe any relationship. However, the LCL over Thiruvananthapuram is found to be higher than the ABL for the majority of the database, in contrast to Gadanki.

Figure 12a and b show the schematic representation of the diurnal evolution of the mean ABL from 11:00 IST on the first day to 11:00 IST on the second day during the winter and summer monsoon seasons, respectively. The diagram is generated from the seasonal mean ABL height data presented in

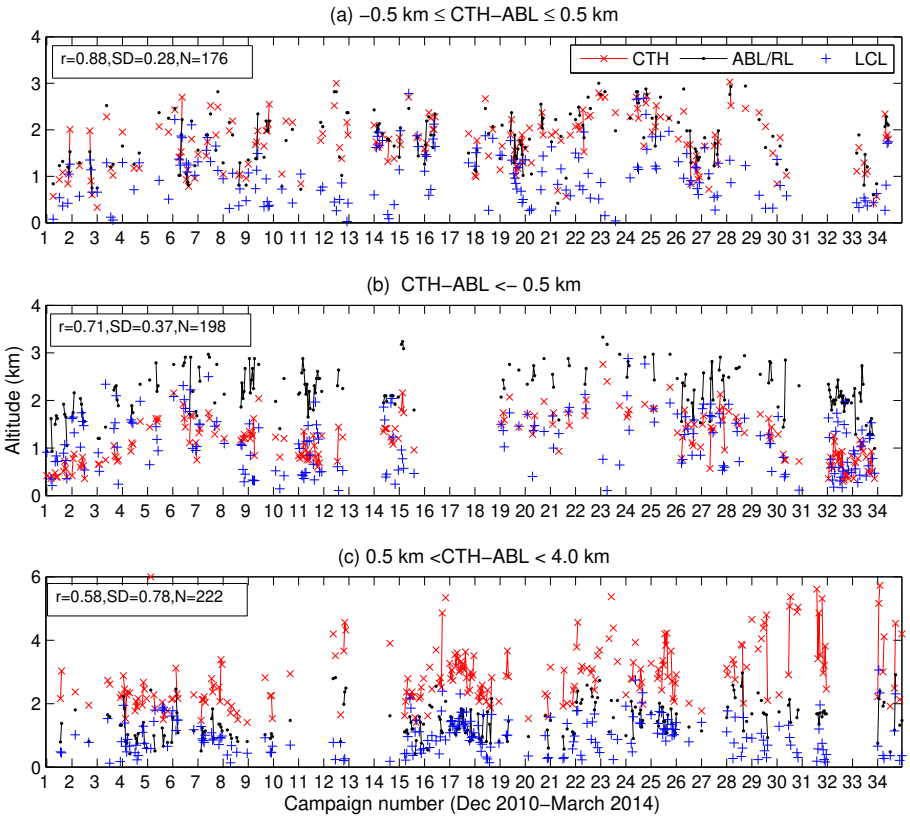

Figure 13. Time series of the CTH, the ABL_{CR} top, and the LCL observed for the cases **(a)** $-0.5\,km \leq CTH–ABL \leq 0.5\,km$, **(b)** $CTH–ABL < -0.5\,km$, and **(c)** $0.5\,km < CTH–ABL < 4.0\,km$.

Fig. 10a and b. The vertical cross section of the ABL characterizing the seasonal mean CBL, SBL, RL, entrainment zone (E.Z.), capping inversion, the LCL, and CTH is generated from the observed data over Gadanki. The schematic diagram represents the typical evolution of the boundary layer, consistent with the diagram presented in the Stull (1988) and Wallace and Hobbs (2006). The CBL during the winter evolves slowly when compared to the summer monsoon season, in which the ABL growth is rapid. The SBL starts to form well before the sunset during both seasons; however, it remains persistent even after the sunrise only during the winter season. During the winter, the RL remains almost constant throughout the night. However, during the summer, the RL rapidly decreases as the night passes. The capping inversion during the summer is thicker when compared to the summer monsoon. We have also shown the seasonal mean LCL and CTH representing the cloud base and top, respectively. The LCL occurs within the CBL and RL during both the seasons. The mean CTH has very little variation over the diurnal cycle during both the seasons. During winter season, the CTH is slightly higher during morning hours between 05:00 and 08:00 IST. It could be due to frequent occurrence of the fogs or stratus clouds in the morning hours during winter season over Gadanki region. Note that the transition regions (from the CBL to RL during ET and the RL to CBL during MT) cannot be accurately represented with available time resolutions. Thus, the part of the CBL after the sunset and the part of the RL after the sunrise may not possess any meaning. This schematic diagram clearly represents the typical (Fig. 4) annual mean (Fig. 9) and seasonal mean (Fig. 10) diurnal characteristic of the ABL.

3.7 Qualitative relationships between CTH and ABL_{CR} height

The presence of clouds has a large impact on the boundary layer structure. However, it leads to considerable complication because of the important role played by radiative fluxes and phase change (Garratt, 1992). The relationship between the CTH and the CBL/RL is obtained and is shown in Fig. 13. We have observed the CTH at various layers ranging from within the ABL to up to 12 km during the different campaigns. The CTH relative to the ABL_{CR} is obtained for each individual campaign, which is listed in Table 1. In total, for 630 cases clouds were present below, near to, or above the ABL_{CR}. The remaining 50 cases are when clear sky conditions were observed. Note that in a total of 680 cases, CBL and RL are defined. We observed that in 175, 199, 222, and 34 cases, CTH occurred within ±0.5 km, below

0.5 km, above 0.5 km but below 6.0 km, and above 6.0 km of the ABL_{CR}, respectively. These cutoff heights regions are selected through visual inspection by trial and error after examining several ABL height and CTH time series. The time series of the CTH, ABL_{CR}, and LCL for the cases when the CTH occurred within ±0.5 km, below 0.5 km, and above 0.5 km but below 6.0 km of ABL_{CR} are shown in Fig. 13. The CTH within ±0.5 km of the ABL_{CR} is positively correlated ($r = 0.88$) with SD of 0.28 km (Fig. 13a). Figure 13a further reveals a clear association between the ABL_{CR} and the CTH variations. These cases indicate the cloud-topped boundary layer where clouds are limited in their vertical extent by main capping or subsidence inversion (Garratt, 1992). Figure 13b shows that the CTH occurring below 0.5 km of the ABL_{CR} is also positively correlated ($r = 0.71$) with SD of 0.37 km. Although these clouds occur well below the ABL_{CR}, both vary in the similar fashion (Fig. 13b). It can be seen that the higher the cloud level is, the higher the ABL_{CR} and vice versa. Similarly, the ABL_{CR} height variation is also well correlated ($r = 0.58$) with the CTH variation occurring above 0.5 km but below 6.0 km of the ABL_{CR} (Fig. 13c).

When the CTH is within ±0.5 km of the ABL_{CR}, LCL occurs mostly below the ABL, except a few cases when it coincides with either the ABL or CTH (Fig. 13a). When the CTH is below 0.5 km of the ABL_{CR}, the LCL again occurs mostly below the ABL but generally coincided with the CTH (Fig. 13b). In this case, the LCL sometimes also occurs above the CTH. Clouds occurring below the ABL could be the shallow clouds; in such cases LCL representing the cloud base may occur near to the CTH. However, it is to be noted that the CTH represents the cloud condition for the area averaged over 0.25° latitude × 0.25° longitude regions, whereas the LCL indicates the cloud base exactly over the observation site. Thus, the LCL may not always agree with the CTH when clouds are not extended over the larger area. For the cases when clouds occurring above 0.5 km but below 6.0 km of the ABL_{CR}, the LCL mostly occurs either below the ABL or generally coincides with the ABL (Fig. 13c).

It is interesting to note that whenever the CTH is below the ABL_{CR}, CBL and RL occur at higher height (mostly above 2 km), whereas whenever the CTH is above the ABL_{CR}, CBL and RL occur at a lower height (mostly below 2.0 km). Generally, the CBL (sometimes also called as fair weather boundary layer) occurs at lower height during a shallow cumulus when compared to clear sky conditions (Medeiros et al., 2005). Very deep convective clouds do not show any relationship with the ABL_{CR} variation (figure not shown) as can be seen from Fig. 4b. Qualitatively, it indicates that the presence of clouds near to the CBL and RL directly impact its variation, but not the high level clouds due to the deep convection events. It is to be noted that there are two occasions when rainfall occurred during the campaign periods, but these few data do not reveal any relation between the ABL and rainfall.

4 Discussion and conclusions

The unique and long-term intensive campaigns of high vertical resolution radiosonde observations on multiple 3 h intervals over a tropical location, Gadanki, in the Indian monsoon region reveal the clear diurnal structure of the ABL height. The high vertical resolution of the radiosonde data enables us to detect the SBL height directly, which would otherwise be very difficult.

Identification of the ABL is generally preferred using θ_v and q obtained from radiosonde observation because they can represent the mixing height better than the T. However, we observed an excellent correlation between T and θ_v suggesting that ABL can be identified using T. Moreover, use of T can give both elevated inversion and SBI and is well suited to study the diurnal variation of the ABL. The limitation of using T is that it can also identify midlevel inversions sometimes. However, to avoid midlevel inversions, if any, we have restricted the ABL height identification below 3.5 km. In case of multiple inversions, the lower one with 80 % of main inversion is considered. The correlation between T (or θ_v) and N is in good agreement with Basha and Ratnam (2009). We also found that N yields the ABL height lower than that of T several times, but not always, in contrast to Chennai, located 120 km southeast of Gadanki, where significant ABL height difference of ∼ 0.84 (between θ and N) is observed in evening soundings (Seidel et al., 2010).

The nighttime ABL is complex to define when compared to daytime ABL. As the nighttime ABL or the SBL depends on the surface cooling, if it delays, or does not form at all, which generally happens, one will find it as about same as pervious daytime ABL (i.e CBL). It is the part of the daytime mean state and has not formed due to action of nighttime surface forcing. However, as it is above the surface, which is the only criterion left to assign the RL as the ABL in the absence of the SBL (Liu and Liang, 2010). However, if the measuring instrument has limited capability to detect the SBL, one will identify the RL as nighttime ABL, which will not be a true representation of the ABL height.

In total, the SBL forms about 50 % of the time from midnight to morning. In the early part of the night, the SBL occurs less frequently (33 %) than late night and hence indicates the delay in the surface cooling process. The SBL forms more frequently during winter season when compared to other seasons. Thus, diurnal variation of the ABL occurs more often during winter than summer. There could be various reasons for the delay in the SBL formation, such as cloud cover or wet surface due to rain, which can disturb or delay the surface cooling process. Sandeep et al. (2015) observed that the ABL over Gadanki after the sunset becomes shallower and its growth delayed by 1–4 h during wet episodes. Over Indian region, clouds and precipitation most frequently occur during the summer monsoon season when compared to the winter season, suggesting the formation of the SBL will be less frequent during the former season, consistent

with the observed result. However, irrespective of the season, the surface temperature shows a diurnal pattern. Thus, another reason for less occurrence of the SBL during summer monsoon season could be high nighttime temperature. In fact the nighttime surface temperatures during summer monsoon as well as post- and pre-monsoons are greater than daytime surface temperature during the winter season. Though the surface temperature during these seasons decreases during nighttime, it does not have a sufficient cooling effect as during the winter season, probably preventing the formation of the SBL most of the time during the summer season. Thus, it could be possible that even though the surface temperatures show diurnal variation during the summer monsoon, diurnal variability in the ABL may not be expected.

The minimum height of the CBL at 08:00 IST is due to weak convection (thermals) during the morning hours when compared to other times of the day. As convection becomes stronger (the strongest surface warming at 14:00 IST) due to the strong thermals, the CBL becomes higher and reaches a maximum height at 14:00–17:00 IST. Similarly, as the night passes, surface cooling becomes stronger (the strongest cooling occurs at 02:00 IST), leading to higher SBL height at 02:00–05:00 IST. The RL remains sometimes at similar height as the CBL in case of very strong gradient in moisture and temperature. However, it generally lowers as time passes during the night, especially during the summer monsoon season. As daytime convection is switched off during the night, the turbulence strength goes weaker and weaker as night passes, leading to a decrease in the RL height.

During the pre-monsoon, the surface temperature has the strongest diurnal variation, which manifests stronger diurnal variation of the ABL_{CR} height (Angevine et al., 2001). However, higher CBL occurs during the summer monsoon season and not during the pre-monsoon. The higher CBL during summer monsoon season is due to stronger convection occurring in this season when compared to the other seasons. During the winter season, the surface temperature is low, leading to a weak diurnal pattern of the ABL_{CR} (Angevine et al., 2001). Since convection is weaker during the winter season, the CBL is at a lower height when compared to the other seasons. The reversal of the CBL and RL height patterns between summer monsoon and winter is due to the surface temperature variation and strength of convection. It is due to the fact that during the winter the RL does not lower as observed for the other seasons due to less surface temperatures, while the CBL becomes higher during summer monsoon seasons due to stronger convection when compared to the winter. Thus, the CBL is lower during the winter but higher during summer monsoon, while RL is higher during the winter but lower during the summer monsoon season.

Finally, the qualitative relationship between the ABL_{CR} height, the CTH, and the LCL is examined. We only provide here qualitative information based on the CTH obtained using merged TBB data, since direct observations of the CTH over the launch site during the campaign periods are not available. As observed in this study, the CTH at various layers has been observed using ceilometer at Ahmedabad (23.03° N 72.54° E), India (Sharma et al., 2016). As suggested by Wang and Rassow (1995), the various cloud layers can be obtained utilizing the RH data. However, as the criteria for fixing the cloud base and top heights using the RH data have not been finalized for the tropical clouds occurring over this region, we have preferred satellite-derived CTH data in this study. We also obtained the LCL height, but for the majority of the database LCL occurs below the ABL and they are randomly related, consistent with Anurose et al. (2016). Thus, we have interpreted our results based on the CTH data only. If clouds occur above the ABL_{CR} during the daytime, they will absorb the incoming solar radiation and hence cool the surface. This in turn will weaken the thermals and hence decrease the CBL height. However, when clouds occur below the CBL, it will cool the surface but warm the region between the cloud top and CBL and hence can strengthen the thermals, which will lead to increase the CBL height. This explains why CBL is at lower height when clouds are above it and at the higher height when clouds are below it. If clouds occur during nighttime, the situation will be more complex and the RL variability will be more difficult to explain. During nighttime, clouds will block the outgoing long-wave radiation, which in general warms below the RL and hence disturbs the surface cooling and the formation of the SBL. The verification of the CTH height using spaceborne satellites and ground-based observations such as ceilometer over the launch site will be carried out as a separate study in the future.

The following are the main findings on the diurnal variability of the ABL:

1. The CBL height has a large variation ranging from as low as 0.4 km to as high as about 3.0 km above the surface and occurs uniformly at 3 h intervals during the diurnal cycle over Gadanki, a tropical station in the Indian monsoon region.

2. The SBL mainly forms during nighttime; however, it can also form during daytime, especially during evening and morning hours, i.e., during transition periods. The SBL forms about 50 % of the time during 23:00–05:00 IST. At 20:00 IST, occurrence of the SBL is only 33 %, indicating a delay in surface cooling about 17 % of the time. About 25 % of the time the SBL forms at 08:00 IST, indicating the dominance of the surface cooling even after the sunrise. As surface cooling starts well before the sunset, sometimes the SBL (about 9 % of the time) also forms at 17:00 IST.

3. The overall mean SBL lies well within the 0.3 km and the mean CBL lies well within 3.0 km, consistent with the available literature. However, the maximum probability distribution of the SBL occurs at 0.15 km lower than its mean value. In contrast to the SBL, the maxi-

mum probability distribution of the CBL coincides with mean CBL at about 2 km for the winter season and the whole year. The maximum probability distribution of the CBL during the summer monsoon season has a broader peak when compare to winter season.

4. The CBL and the RL heights obtained using different methods (T, θ_v, q, and N) correlate well.

5. A clear diurnal variation of the ABL_{CS} height over the different seasons is observed with the maximum CBL height during the summer monsoon season while the maximum SBL height is seen during the winter to pre-monsoon. The seasonal pattern reverses for the RL height that becomes higher during the winter and lower during the summer monsoon season.

6. The ABL_{CR} height is positively correlated with the CTH occurring near to it; however, the deep convective clouds do not show any relationship. When clouds are at lower height the ABL_{CR} is relatively higher and vice versa. This needs to be verified using independent observations of the CTH perhaps using ceilometer observations.

7. Over Gadanki, the LCL occurs below the CBL and RL for the majority of the database and they are randomly related.

5 Data availability

The radiosonde data used in this study are not open for public yet. However, the data can be provided upon request to either M. Venkat Ratnam (vratnam@narl.gov.in) or the corresponding author.

The Supplement related to this article is available online at doi:10.5194/acp-17-531-2017-supplement.

Acknowledgements. We thank NARL radiosonde operation team for conducting the experiment under tropical tropopause dynamics (TTD) campaigns fully supported by the Indian Space Research Organization as a part of CAWSES India Phase-II program. We also thank two reviewers and the editor for valuable comments and suggestions. All figures are generated using MATLAB software. This work is partially supported by network projects under Earth Science Technology Cell (ESTC) under Ministry of Earth Sciences (MoES) and Department of Science and Technology-Science and Engineering Research Board (EMR/2015/000525).

Edited by: H. Wang
Reviewed by: two anonymous referees

References

Angevine, W. M., Baltink, H. K., and Bosveld, F. C.: Observations of the morning transition of the convective boundary layer, Bound.-Lay. Meteorol., 101, 209–227, 2001.

Anurose, T. J., Subrahamanyam, D. B., and Sunilkumar, S. V.: Two years observations on the diurnal evolution of coastal atmospheric boundary layer features over Thiruvananthapuram (8.5° N, 76.9° E), India, Theor. Appl. Climatol., doi:10.1007/s00704-016-1955-y, 2016.

Ao, C. O., Waliser, D. E., Chan, S. K., Li, J. L., Tian, B., Xie, F., and Mannucci, A. J.: Planetary boundary layer heights from GPS radio occultation refractivity and humidity profiles, J. Geophys. Res.-Atmos., 117, D16117, doi:10.1029/2012JD017598, 2012.

Basha, G. and Ratnam, M. V.: Identification of atmospheric boundary layer height over a tropical station using high-resolution radiosonde refractivity profiles: Comparison with GPS radio occultation measurements, J. Geophys. Res.-Atmos., 114, D16101, doi:10.1029/2008JD011692, 2009.

Bianco, L., Djalalova, I., King, C., and Wilczak, J.: Diurnal evolution and annual variability of boundary-layer height and its correlation to other meteorological variables in California's Central Valley, Bound.-Lay. Meteorol., 140, 491–511, 2011.

Bolton, D.: The computation of equivalent potential temperature, Mon. Weather Rev., 108, 1046–1053, 1980.

Brill, K. and Albrecht, B.: Diurnal variation of the trade-wind boundary layer, Mon. Weather Rev., 110, 601–613, 1982.

Chan, K. M. and Wood, R.: The seasonal cycle of planetary boundary layer depth determined using COSMIC radio occultation data, J. Geophys. Res.-Atmos., 118, 12422–12434, doi:10.1002/2013JD020147, 2013.

Chandrasekhar Sarma, T. V., Narayana Rao, D., Furumoto, J., and Tsuda, T.: Development of radio acoustic sounding system (RASS) with Gadanki MST radar – first results, Ann. Geophys., 26, 2531–2542, doi:10.5194/angeo-26-2531-2008, 2008.

Clifford, S. F., Chandran Kaimal, J., Lataitis, R. J., and Strauch, R. G.: Ground-based remote profiling in atmospheric studies: An overview, Proc. IEEE, 82, 313–355, 1994.

Deardorff, J. W.: Parameterization of the planetary boundary layer for use in general circulation models 1, Mon. Weather Rev., 100, 93–106, 1972.

Garratt, J.: The atmospheric boundary layer, Cambridge atmospheric and space science series, Cambridge University Press, Cambridge, 316 pp., 1992.

Garratt, J. R.: Review: the atmospheric boundary layer, Earth-Sci. Rev., 37, 89–134, 1994.

Hashiguchi, H., Yamanaka, M. D., Tsuda, T., Yamamoto, M., Nakamura, T., Adachi, T., Fukao, S., Sato, T., and Tobing, D. L.: Diurnal variations of the planetary boundary layer observed with anL-band clear-air doppler radar, Bound.-Lay. Meteorol., 74, 419–424, 1995a.

Hashiguchi, H., Fukao, S., Tsuda, T., Yamanaka, M. D., Tobing, D. L., Sribimawati, T., Harijono, S. W. B., and Wiryosumarto, H.: Observations of the planetary boundary layer over equatorial Indonesia with an L band clear-air Doppler radar: Initial results, Radio Sci., 30, 1043–1054, 1995b.

Holtslag, A. and Nieuwstadt, F.: Scaling the atmospheric boundary layer, Bound.-Lay. Meteorol., 36, 201–209, 1986.

Konor, C. S., Boezio, G. C., Mechoso, C. R., and Arakawa, A.: Parameterization of PBL processes in an atmospheric general cir-

culation model: description and preliminary assessment, Mon. Weather Rev., 137, 1061–1082, 2009.

Kumar, K. K. and Jain, A.: L band wind profiler observations of convective boundary layer over Gadanki, India (13.5° N, 79.2° E), Radio Sci., 41, RS2004, doi:10.1029/2005RS003259, 2006.

Kumar, M. S., Anandan, V., Rao, T. N., and Reddy, P. N.: A climatological study of the nocturnal boundary layer over a complex-terrain station, J. Appl. Meteorol. Clim., 51, 813–825, 2012.

Liu, S. and Liang, X.-Z.: Observed diurnal cycle climatology of planetary boundary layer height, J. Climate, 23, 5790–5809, 2010.

May, P. T., Long, C. N., and Protat, A.: The diurnal cycle of the boundary layer, convection, clouds, and surface radiation in a coastal monsoon environment (Darwin, Australia), J. Climate, 25, 5309–5326, 2012.

Medeiros, B., Hall, A., and Stevens, B.: What controls the mean depth of the PBL?, J. Climate, 18, 3157–3172, 2005.

Mehta, S. K., Ratnam, M. V., and Krishna Murthy, B.: Multiple tropopauses in the tropics: A cold point approach, J. Geophys. Res.-Atmos., 116, D20105, doi:10.1029/2011JD016637, 2011.

Ratnam, M. V., Sunilkumar, S., Parameswaran, K., Murthy, B. K., Ramkumar, G., Rajeev, K., Basha, G., Babu, S. R., Muhsin, M., and Mishra, M. K.: Tropical tropopause dynamics (TTD) campaigns over Indian region: An overview, J. Atmos. Sol.-Terr. Phy., 121, 229–239, 2014.

Sandeep, A., Rao, T. N., and Rao, S. V. B.: A comprehensive investigation on afternoon transition of the atmospheric boundary layer over a tropical rural site, Atmos. Chem. Phys., 15, 7605–7617, doi:10.5194/acp-15-7605-2015, 2015.

Santanello Jr., J. A., Friedl, M. A., and Ek, M. B.: Convective planetary boundary layer interactions with the land surface at diurnal time scales: Diagnostics and feedbacks, J. Hydrometeorol., 8, 1082–1097, 2007.

Schmid, P. and Niyogi, D.: A Method for Estimating Planetary Boundary Layer Heights and Its Application over the ARM Southern Great Plains Site, J. Atmos. Ocean. Technol., 29, 316–322, 2012.

Seibert, P., Beyrich, F., Gryning, S.-E., Joffre, S., Rasmussen, A., and Tercier, P.: Review and intercomparison of operational methods for the determination of the mixing height, Atmos. Environ., 34, 1001–1027, 2000.

Seidel, D. J., Ao, C. O., and Li, K.: Estimating climatological planetary boundary layer heights from radiosonde observations: Comparison of methods and uncertainty analysis, J. Geophys. Res.-Atmos., 115, D16113, doi:10.1029/2009JD013680, 2010.

Seidel, D. J., Zhang, Y., Beljaars, A., Golaz, J. C., Jacobson, A. R., and Medeiros, B.: Climatology of the planetary boundary layer over the continental United States and Europe, J. Geophys. Res.-Atmos., 117, D17106, doi:10.1029/2012JD018143, 2012.

Sharma, S., Vaishnav, R., Shukla, M. V., Kumar, P., Kumar, P., Thapliyal, P. K., Lal, S., and Acharya, Y. B.: Evaluation of cloud base height measurements from Ceilometer CL31 and MODIS satellite over Ahmedabad, India, Atmos. Meas. Tech., 9, 711–719, doi:10.5194/amt-9-711-2016, 2016.

Shravan Kumar, M. and Anandan, V.: Comparision of the NCEP/NCAR Reanalysis II winds with those observed over a complex terrain in lower atmospheric boundary layer, Geophys. Res. Lett., 36, L01805, doi:10.1029/2008GL036246, 2009.

Sokolovskiy, S., Kuo, Y. H., Rocken, C., Schreiner, W., Hunt, D., and Anthes, R.: Monitoring the atmospheric boundary layer by GPS radio occultation signals recorded in the open-loop mode, Geophys. Res. Lett., 33, L12813, doi:10.1029/2006GL025955, 2006.

Stull, R. B.: An introduction to boundary layer meteorology, Atmospheric Sciences Library, Dordrecht, Kluwer, 670 pp., 1988.

Tucker, S. C., Senff, C. J., Weickmann, A. M., Brewer, W. A., Banta, R. M., Sandberg, S. P., Law, D. C., and Hardesty, R. M.: Doppler lidar estimation of mixing height using turbulence, shear, and aerosol profiles, J. Atmos. Ocean. Technol., 26, 673–688, 2009.

van der Kamp, D. and McKendry, I.: Diurnal and seasonal trends in convective mixed-layer heights estimated from two years of continuous ceilometer observations in Vancouver, BC, Bound.-Lay. Meteorol., 137, 459–475, 2010.

Wallace J. M. and Hobbs, P. V.: Atmospheric science an introductory survey, second edition. International Geophysics series, Acadamic Press, 92, 483 pp., 2006.

Wang, J. and Rossow, W. B.: Determination of cloud vertical structure from upper-air observations, J. Appl. Meteorol., 34, 2243–2258, 1995.